

Article

Not peer-reviewed version

---

# Is the Hyperscaling Relation Violated Below the Upper Critical Dimension in Some Particular Cases?

---

[Hung T. Diep](#)<sup>\*</sup> and Van Thanh Ngo

Posted Date: 24 February 2025

doi: 10.20944/preprints202502.1793.v1

Keywords: Critical Exponents; Thin Films; Hyperscaling Relations; Effective Dimension; Multi-Histogram Monte Carlo Technique



Preprints.org is a free multidisciplinary platform providing preprint service that is dedicated to making early versions of research outputs permanently available and citable. Preprints posted at Preprints.org appear in Web of Science, Crossref, Google Scholar, Scilit, Europe PMC.

Copyright: This open access article is published under a Creative Commons CC BY 4.0 license, which permit the free download, distribution, and reuse, provided that the author and preprint are cited in any reuse.

Article

# Is the Hyperscaling Relation Violated Below the Upper Critical Dimension in Some Particular Cases?

Hung T. Diep<sup>1,\*</sup>  and Van-Thanh Ngo<sup>2</sup>

<sup>1</sup> Laboratoire de Physique Théorique et Modélisation, CY Cergy Paris Université (Formerly, University of Cergy-Pontoise), CNRS, UMR 8089, 2 Avenue Adolphe Chauvin, 95302 Cergy-Pontoise, France

<sup>2</sup> Institute of Scientific Data and Information, Vietnam Academy of Science and Technology (VAST), 18 Hoang Quoc Viet, Hanoi 10000, Vietnam

\* Correspondence: diep@cyu.fr

**Abstract:** In this review, we show our results with new interpretation on the critical exponents of thin films obtained by high-performance multi-histogram Monte Carlo simulations. The film thickness  $N_z$  consists of a few layers up to a dozen of layers in the  $z$  direction. The free boundary condition is applied in this direction while in the  $xy$  plane periodic boundary conditions are used. The large  $xy$  plane size, from  $70^2$  to  $160^2$ , is used for finite-size scaling. The Ising model is used with nearest-neighbor (NN) interaction. When  $N_z = 1$ , namely the two-dimensional (2D) system, we find strictly the critical exponents given by the renormalization group. While, for  $N_z > 1$ , the critical exponents calculated with the high-precision multi-histogram technique show that they deviate systematically from the 2D values and get closer to the 3D critical exponents for  $N_z > 13$ . If we argue that as long as the thickness  $N_z$  is small enough, the correlation length in the  $z$  direction is finite, it does not affect the nature of the phase transition, namely it remains in the 2D universality class. This argument is in contradiction with our numerical results which show a systematic deviation from 2D values: If we use these values of critical exponents in the hyperscaling relation with  $d = 2$ , then the hyperscaling relation is violated. However, if we use the hyperscaling relation and the critical exponents obtained for  $N_z > 1$  to calculate the dimension of the system, we find the system dimension between 2 and 3. This can be viewed as an "effective" dimension. More discussion is given in the paper. We also show the cross-over between the first- and second-order transition while varying the film thickness. In addition, we will show evidence that when a 2D system has two order-parameters of different symmetries with a single transition, the critical exponents are new, suggesting a universality class of coupled two-symmetry breakings. In this case, the 2D hyperscaling does not hold. Another case is the 3D Ising model coupled to the lattice vibration: the critical exponents deviate from the 3D Ising ones, the results suggest the violation of the hyperscaling.

**Keywords:** critical exponents; thin films; hyperscaling relations; effective dimension; multi-histogram monte carlo technique

## 1. Introduction

The study of phase transitions is one of the most important tasks in theory, in experiments and in computer simulations since the second half of the 20th century. The main reason is that, if we know the characteristics of a phase transition, we can understand the interaction mechanisms lying behind the transition and we can deduce various physical quantities. Therefore, comparisons between theories, experiments and computer simulations are necessary in order to obtain conclusions. While comparison with experiments is always a challenge because real materials may contain ill-controlled elements such as dislocations, defects and impurities, comparisons between theories and simulations are in most cases possible. This is the purpose of the present short review based on our own works in the past years.

Let us recall that the phase transition was first studied by the mean-field approximation with several improved versions in the 40s (see the textbook [1] where these methods are shown and commented). These were followed by exact-solution methods in two dimensions (2D) such as the Ising model, Potts models and vertex models (see the book by R. Baxter [2]). The break-through in general dimensions come in 1970 with the formulation of the renormalization group by K. G. Wilson [3,4] followed by investigations on the finite-size scaling analysis and their validity [5]. The present Special Issue (SI) revisits the progress made on the scaling and hyperscaling relations above the upper critical dimension  $d_u = 4$ . Several papers in this SI recall the foundation of these relations in a general  $d$ . The reader is referred, for example, to the review by A. Peter Young [6] for a recall of the demonstration of these relations (see also the review by Honchar et al. [7]). The main question of this SI is whether or not the hyperscaling is violated for dimension  $d$  larger than the upper critical dimension  $d_u = 4$ . However, we show that the question of the violation of the hyperscaling is also posed in  $d < 4$  in some specific cases that we will present in this paper.

The first case concerns the critical exponents obtained by using the highly-precise multi-histogram Monte Carlo (MC) technique [8–10] for a thin film of simple cubic structure with Ising spin model. The film surface  $L^2$  ( $xy$  plane) is very large, up to  $L^2 = 160^2$  lattice sites for some cases, with periodic boundary conditions, while the film thickness  $N_z$  goes from one layer (2D) to 13 layers with free boundary conditions. Finite-size scaling (FSS) has been used with varying  $L$  to calculate the critical exponents. These results have been published in Ref. [11] but the aspect of the violation of the hyperscaling relation has not been discussed. In the light of the topic of the present Special Issue, we revise the interpretation of our results. In addition, we review some other cases that we have investigated.

Except the case  $N_z = 1$ , the question on the dimension of the system is naturally arised. For Capehart and Fisher [12], there is a cross-over from 2D to 3D when  $N_z$  is increased. So, how to use the hyperscaling relation, namely with which dimension ? We will discuss in this paper.

This short review is organized as follows. Section 2 is devoted to the case of thin films mentioned above where the multi-histogram technique is recalled. Section 3 shows the results of critical exponents obtained with the FSS. Section 4 reviews the case of a cross-over between the first- and second-order transitions when the film thickness is decreased. Section 5 is devoted to some other cases where the hyperscaling relation is violated or seems to be violated. Concluding remarks are given in section 6.

## 2. Critical Behavior of Thin Films

### 2.1. Model

We consider a thin film composing of  $N_z$  layers of  $xy$  square lattices stacking in the  $z$  direction. The  $xy$  plane has the dimension  $L \times L$  where  $L$  is the linear dimension. We use a simple Hamiltonian which consists of Ising spins occupying the lattice sites. The spins interact with each other via an exchange interaction  $J$  between nearest neighbors (NN). We assume  $J$  to be unique everywhere including between surface spins. The Hamiltonian is written as

$$\mathcal{H} = -J \sum_{i,j} \sigma_i \sigma_j \quad (1)$$

In the simulations which will be shown below, we take  $N_z$  from 1 to 13 and  $L = 20 - 80$  (for some cases  $L$  is up to 160). Before showing our results, let us summarize the multi-histogram technique in the following.

### 2.2. Multi-Histogram Technique

The principle of a single histogram MC method is to record the energy histogram  $H(E)$  collected at a temperature  $T$  as close as possible to the transition temperature obtained from the standard MC simulation. From  $H(E)$  one can calculate thermodynamic quantities using formulas of the canonical distribution. The error depends on how far the chosen temperature is from the transition temperature

$T_c$ . Multi-histogram technique helps overcome this uncertainty. We know that with a finite-size system the maximum of the specific heat  $C_v$  and the maximum of the susceptibility  $\chi$  do not occur at the same temperature. In the multi-histogram technique, we take another temperature close to the maximum of  $C_v$  and the maximum of  $\chi$  to calculate by histogram technique the new temperatures of the maxima of  $C_v$  and  $\chi$ . We repeat again this procedure for 8 temperatures: such an iteration procedure improves the positions of the maxima of  $C_v$  and  $\chi$  at the system size  $(L, N_z)$ .

The reader is referred to Refs. [9,11] for the technical details.

Note that, as in the single histogram technique, thermal physical quantities are calculated as continuous functions of  $T$  which allow for the precise determination of the peak positions and the peak heights of  $C_v$  and  $\chi$  for a given system size. This permits to make the finite-size scaling with precision. In addition, since we take many temperatures in the transition region, the results obtained by multi-histogram method are valid for a wider range of temperature, unlike a single histogram technique with the results valid only in a very small temperature region, typically  $[T - T_c(\infty)]/T_c(\infty) \simeq \pm 1\%$ .

In MC simulations, we calculate the thermal averages of

- the magnetization  $\langle M \rangle$

$$\langle M \rangle = \frac{1}{L^2 N_z} \left\langle \sum_i \sigma_i \right\rangle \quad (2)$$

- the total energy  $\langle E \rangle$ ,

$$\langle E \rangle = \langle \mathcal{H} \rangle, \quad (3)$$

- the heat capacity  $C_v$ ,

$$C_v = \frac{1}{k_B T^2} \left( \langle E^2 \rangle - \langle E \rangle^2 \right), \quad (4)$$

- the susceptibility  $\chi$ ,

$$\chi = \frac{1}{k_B T} \left( \langle M^2 \rangle - \langle M \rangle^2 \right), \quad (5)$$

- the Binder energy cumulant  $U$ ,

$$U = 1 - \frac{\langle E^4 \rangle}{3 \langle E^2 \rangle^2}, \quad (6)$$

-  $n^{\text{th}}$  order cumulant of the order parameter  $V_n$  for  $n = 1$  and 2:

$$V_n = \frac{\partial \ln M^n}{\partial (1/k_B T)} = \langle E \rangle - \frac{\langle M^n E \rangle}{\langle M^n \rangle}. \quad (7)$$

Note that if we scale with  $L$ , we have the following relations, since  $N_z$  is fixed [6,9,13]:

$$V_1^{\max} \propto L^{1/\nu}, \quad V_2^{\max} \propto L^{1/\nu}, \quad (8)$$

$$C_v^{\max} = C_0 + C_1 L^{\alpha/\nu} \quad (9)$$

and

$$\chi^{\max} \propto L^{\gamma/\nu} \quad (10)$$

at their respective 'transition' temperatures  $T_c(L)$ , and

$$U = U[T_c(\infty)] + A L^{-\alpha/\nu}, \quad (11)$$

$$M_{T_c(\infty)} \propto L^{-\beta/\nu} \quad (12)$$

and

$$T_c(L) = T_c(L = \infty) + C_A L^{-1/\nu} \quad (13)$$

In the above relations,  $A$ ,  $C_0$ ,  $C_1$  and  $C_A$  are constants. The exponent  $\nu$  can be calculated by Eqs. (8). For  $L$  large enough,  $V_1^{\max}$  and  $V_2^{\max}$  should give the same  $\nu$  as seen below. Then, from Eq. (13) we

estimate  $T_c(L = \infty)$ . Using this, we calculate  $\alpha$  and  $\beta$  from Eqs. (11) and (12). We will check the Rushbrooke inequality  $\alpha + 2\beta + \gamma \geq 2$  and the hyperscaling relation  $d\nu = 2 - \alpha$  in the following.

To ensure that Eqs. (8)-(13) are used for  $L$  large enough, one uses the following corrections to scaling of the form

$$\chi^{\max} = B_1 L^{\gamma/\nu} (1 + B_2 L^{-\omega}) \quad (14)$$

$$V_n^{\max} = D_1 L^{1/\nu} (1 + D_2 L^{-\omega}) \quad (15)$$

$B_1, B_2, D_1$  and  $D_2$  being constants and  $\omega$  a correction exponent.[14] Normally, if  $L$  is large enough, the corrections are very small. With today's computer-memory capacity, large  $L$  is often used as seen below. The scaling corrections are thus extremely small, they do not therefore alter the results using Eqs. (8)-(13).

### 3. Results

Most of the results shown below have been published by us in [11]. However, in light of the new interpretation on the violation of the hyperscaling relation, we review them here to show that there is a possibility that the hyperscaling relation  $d\nu = 2 - \alpha$  is violated below  $d_u$ : as said in the Introduction, in the case of thin films where the thickness is finite and small, the hyperscaling relation is satisfied only when  $d$  has a value between 2 and 3. This non-integer dimension is called by Capehart and Fisher [12] "cross-over dimension". To our knowledge,  $d$  in the hyperscaling relation is the space dimension, it is 2, 3, ... (integer), it cannot be between 2 and 3. We are convinced that the hyperscaling relation may not be valid in the case of thin films shown below and in other particular cases shown in section 5.

First, we show the layer magnetizations and their corresponding susceptibilities of the first three layers in the case where  $N_z = 5, L = 24$  in Figure 1. The layer susceptibilities have their peaks at the same temperature, indicating a single transition. We note that the magnetization is lowest at the surface and increases while going to the interior. This is known a long time ago by the Green's function method [15,16] and by more recent works on thin films with competing interactions [17] and films with Dzyaloshinskii-Moriya interaction [18,19]. Physically, the surface spins have smaller local field due to the lack of neighbors, so thermal fluctuations will reduce more easily the surface magnetization with respect to the interior ones.

We plot in Figure 2 the total magnetization and the total susceptibility. The latter shows only one peak, signature of a single transition. This justifies the study shown below on the criticality of the film transition.

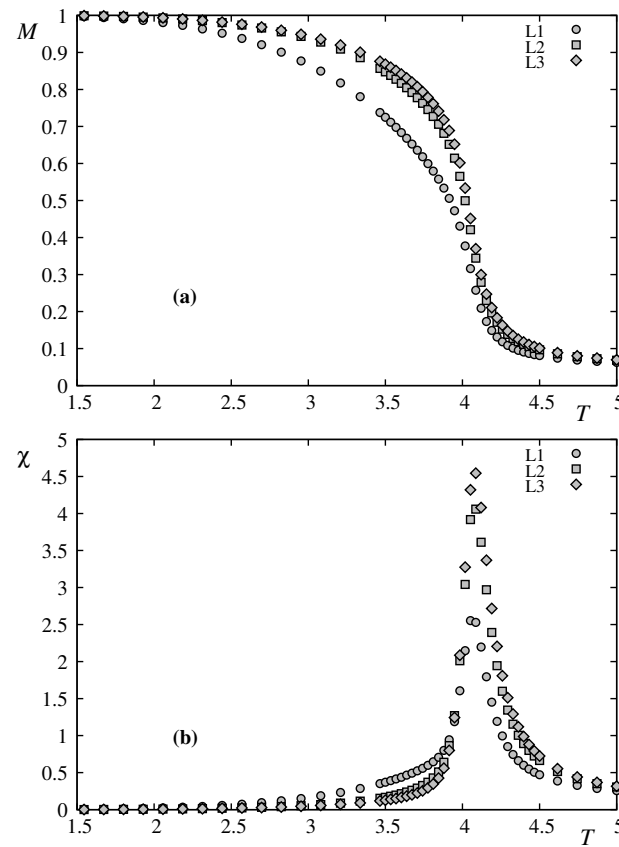


**Figure 1.** (a) Layer magnetizations of layer 1 ( $L_1$ ), layer 2 ( $L_2$ ) and layer 3 ( $L_3$ ) (b) Layer susceptibilities, as functions of  $T$  with  $N_z = 5$  and  $L = 24$ .

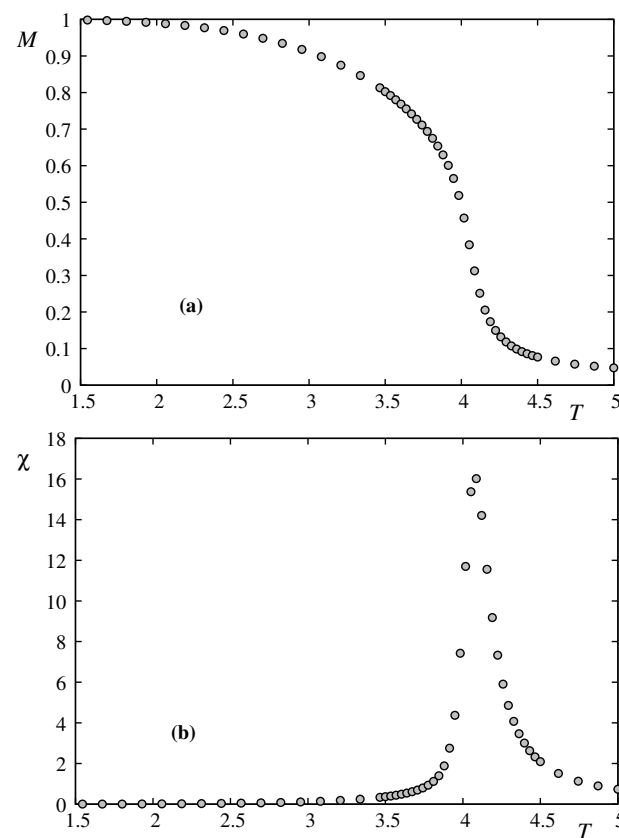


**Figure 2.** (a) Total magnetization, (b) Total susceptibility, versus  $T$  with  $N_z = 5$  and  $L = 24$ .

### 3.1. Finite Size Scaling

Let us show our finite-size scaling (FSS) with  $L$  varying from 20 to 80. For  $N_z = 3$  we use  $L$  up to 160 to evaluate the corrections to scaling.

The technical details can be seen in [11]. We just summarize here: for a given  $N_z$  we use first the standard MC simulations to determine for each size the peak temperatures  $T_c(C_v, L)$  of  $C_v(L)$  and  $T_c(\chi, L)$  of  $\chi(L)$ . The equilibrating time is from 200000 to 400000 MC steps/spin and the averaging time is from 500000 to 1000000 MC steps/spin. Next, as said earlier, we record the energy histograms at 8 different temperatures  $T_j(L)$  around the transition temperatures  $T_c(C_v, L)$  and  $T_c(\chi, L)$  with 2 millions MC steps/spin, after discarding 1 millions MC steps/spin for equilibrating. Such an iteration procedure gives extremely good results. Errors shown in the following have been estimated using statistical errors, which are very small thanks to our multiple histogram procedure, and fitting errors given by fitting software.

### 3.2. Critical Exponents Obtained with Finite-Size Scaling

We show first the peak height of the susceptibility and the maximum of  $V_1$  as functions of  $T$  for varying  $L$  from 20 to 80 in Figure 3.

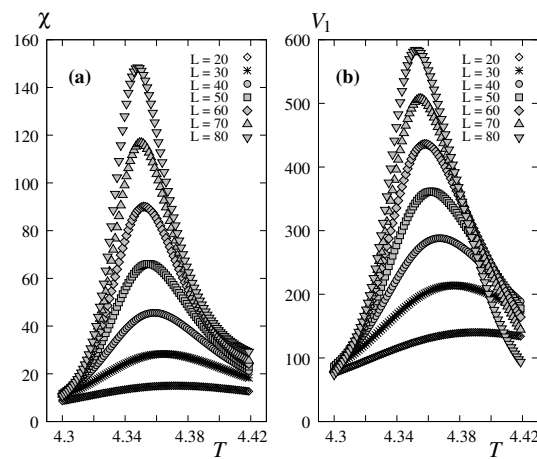


**Figure 3.** (a) Susceptibility and (b)  $V_1$ , as functions of  $T$  for  $L = 20, 30, \dots, 80$  with  $N_z = 11$ , obtained by multiple histogram technique.

Note that the results shown below are obtained using  $T_c(L = \infty, N_z)$  as said earlier below Eq. (13).

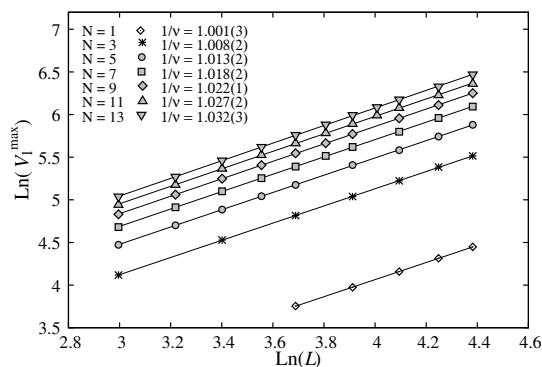


**Figure 4.** Maximum of  $V_1$  versus  $L$  in the  $\ln - \ln$  scale. The slopes are indicated on the figure.

Exponent  $\nu$  is shown as a function of  $N_z$  in Figure 5

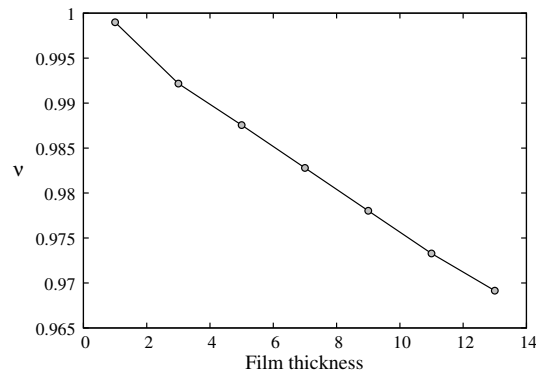


**Figure 5.** Exponent  $\nu$  versus  $N_z$ .

To show the precision of our method, we give here the results of  $N_z = 1$ . For  $N_z = 1$ , we have  $1/\nu = 1.0010 \pm 0.0028$  which yields  $\nu = 0.9990 \pm 0.0031$  and  $\gamma/\nu = 1.7537 \pm 0.0034$  and  $\gamma = 1.7520 \pm 0.0062$ . These results are in excellent agreement with the exact results  $\nu_{2D} = 1$  and  $\gamma_{2D} = 1.75$ . The very high precision of our method is thus verified in the rather modest range of the system sizes  $L = 20 - 80$  used in the present work. Note that the result of Ref.[20] gave  $\nu = 0.96 \pm 0.05$  for  $N_z = 1$  which is very far from the exact value.

The results of  $\gamma/\nu$  are shown in Figures 6 and 7. The results of  $\alpha/\nu$  are shown in Figure 8

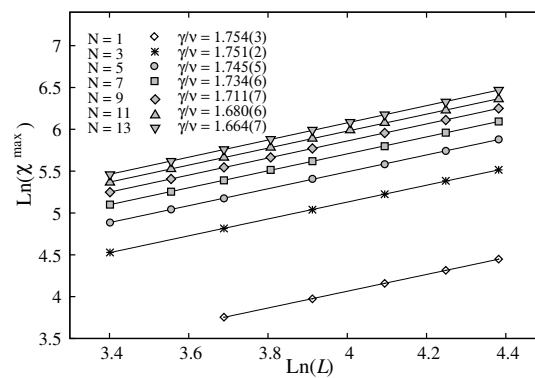


**Figure 6.** Maximum of susceptibility versus  $L$  in the  $\ln - \ln$  scale. The slopes give  $\gamma/\nu$  indicated on the figure.

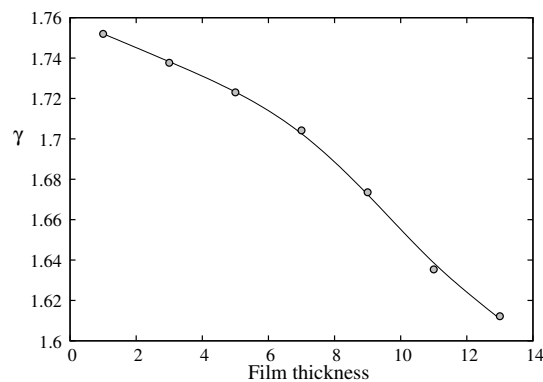


**Figure 7.** Exponent  $\gamma$  versus  $N_z$ .

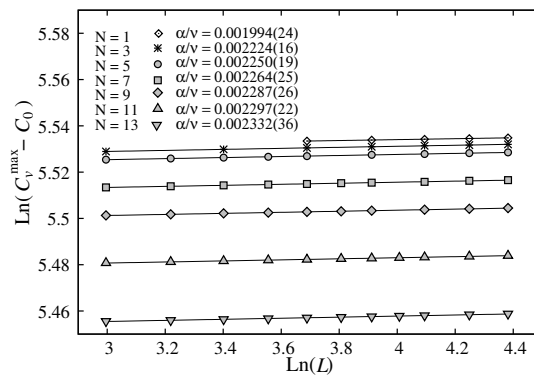


**Figure 8.**  $\ln(C_v^{\max} - C_0)$  versus  $\ln L$  for  $N_z = 1, 3, 5, \dots, 13$ . The slope gives  $\alpha/\nu$  (see Eq. 9) indicated on the figure.

### 3.3. Corrections to Scaling

Let us touch upon the question of corrections to scaling said earlier. We show now that the corrections to scaling are very small.

We consider here the effects of larger  $L$  and of the correction to scaling for  $N_z = 1, 3, \dots, 13$ . The results indicate that larger  $L$  does not change the results shown above. Figure 9(a) displays the maximum of  $V_1$  as a function of  $L$  up to 160. Using Eq. (8), i. e. without correction to scaling, we obtain  $1/\nu = 1.009 \pm 0.001$  which is to be compared to  $1/\nu = 1.008 \pm 0.002$  using  $L$  up to 80. The change is therefore insignificant because it is at the third decimal i. e. at the error level. The same is observed for  $\gamma/\nu$  as shown in Figure 9(b):  $\gamma/\nu = 1.752 \pm 0.002$  using  $L$  up to 160 instead of  $\gamma/\nu = 1.751 \pm 0.002$  using  $L$  up to 80.

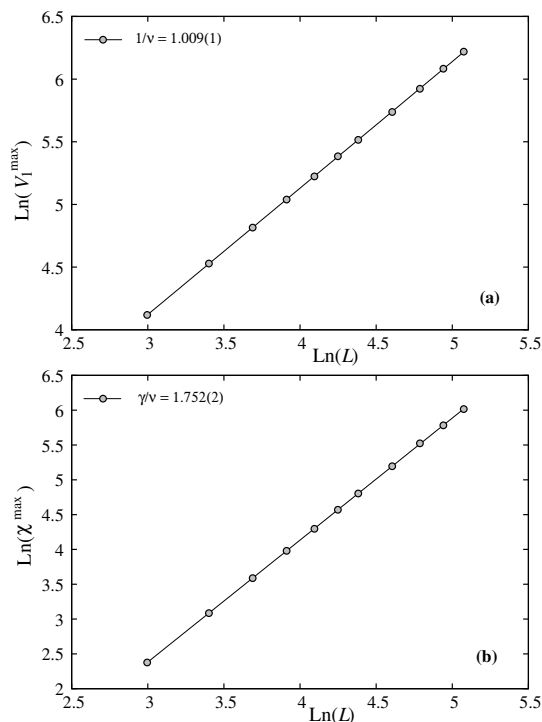


**Figure 9.** (a)  $V_1^{\max}$  and (b)  $\chi_1^{\max}$  vs  $L$  up to 160 with  $N_z = 3$ .

Now, let us allow for correction to scaling, i. e. we use Eq.(14) instead of Eq. (10) for fitting. We obtain the following values:  $\gamma/\nu = 1.751 \pm 0.002$ ,  $B_1 = 0.05676$ ,  $B_2 = 1.57554$ ,  $\omega = 3.26618$  if we use  $L = 70$  to 160 (see Figure 10). The value of  $\gamma/\nu$  in the case of no scaling correction is  $1.752 \pm 0.002$ . Therefore, we can conclude that this correction is insignificant. The large value of  $\omega$  explains the smallness of the correction.

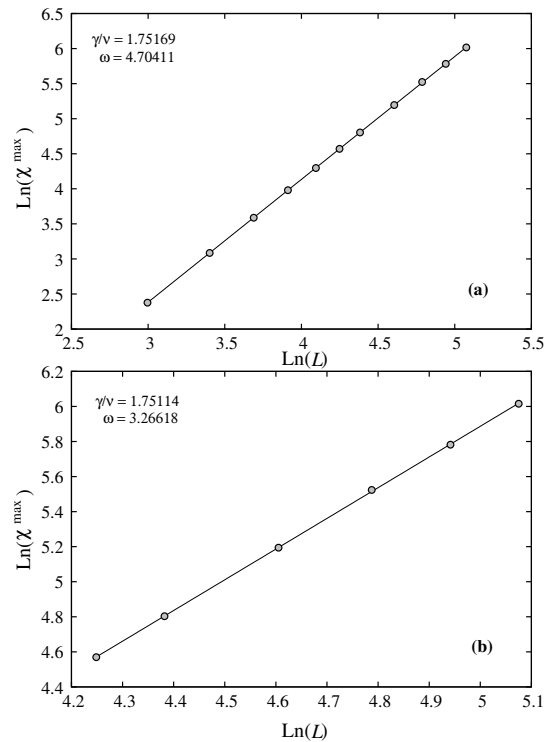


**Figure 10.**  $\chi^{\max}$  vs  $L$  (a) from 20 up to 160 (b) from 70 up to 160, for  $N_z = 3$ .

For  $\beta$ , using Eq. (12) we calculate  $\beta/\nu$  for each thickness  $N_z$ . The results are precise. For example for  $N_z=1$ , we obtained  $\beta/\nu = 0.1268 \pm 0.0022$  which yields  $\beta = 0.1266 \pm 0.0049$  which is in agreement within errors with the exact result  $\beta = 1.25$ . We show in Figure 11 the exponent  $\beta$  versus  $N_z$ .

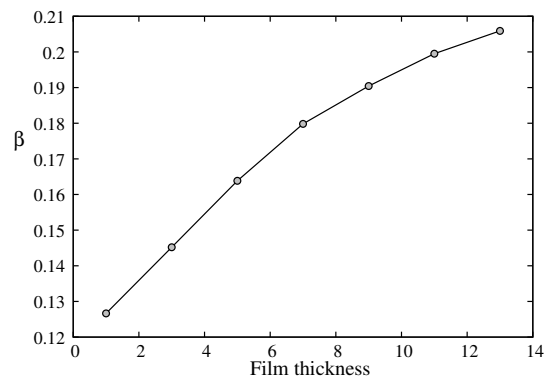


**Figure 11.** Exponent  $\beta$  as a function of the film thickness.

### 3.4. Summary of Our Results

We summarize our results in Table 1. Note that if we use  $\nu$  and  $\alpha$  for a given  $N_z$ , except the case  $N_z = 1 (d = 2)$ , the hyperscaling relation  $d\nu = 2 - \alpha$  is violated if  $d = 2$ . This relation is obeyed if the dimension is replaced by an "effective dimension"  $d_{\text{eff}}$  listed in Table 1 which is larger than 2. The last column shows the critical temperature at  $L = \infty$  obtained by using Eq. (13).

**Table 1.** Critical exponents obtained by multi-histogram technique. The effective dimension and critical temperature  $T_c(L = \infty, N_z)$  are listed in the last two columns. See text for the definition of the effective dimension  $d_{\text{eff}}$ .

$N_z$	$\nu$	$\gamma$	$\alpha$	$\beta$	$d_{\text{eff}}$	$T_c(L = \infty, N_z)$
1	$0.9990 \pm 0.0028$	$1.7520 \pm 0.0062$	$0.00199 \pm 0.00279$	$0.1266 \pm 0.0049$	$2.0000 \pm 0.0028$	$2.2699 \pm 0.0005$
3	$0.9922 \pm 0.0019$	$1.7377 \pm 0.0035$	$0.00222 \pm 0.00192$	$0.1452 \pm 0.0040$	$2.0135 \pm 0.0019$	$3.6365 \pm 0.0024$
5	$0.9876 \pm 0.0023$	$1.7230 \pm 0.0069$	$0.00222 \pm 0.00234$	$0.1639 \pm 0.0051$	$2.0230 \pm 0.0023$	$4.0234 \pm 0.0028$
7	$0.9828 \pm 0.0024$	$1.7042 \pm 0.0087$	$0.00223 \pm 0.00238$	$0.1798 \pm 0.0069$	$2.0328 \pm 0.0024$	$4.1939 \pm 0.0032$
9	$0.9780 \pm 0.0016$	$1.6736 \pm 0.0084$	$0.00224 \pm 0.00161$	$0.1904 \pm 0.0071$	$2.0426 \pm 0.0016$	$4.2859 \pm 0.0022$
11	$0.9733 \pm 0.0025$	$1.6354 \pm 0.0083$	$0.00224 \pm 0.00256$	$0.1995 \pm 0.0088$	$2.0526 \pm 0.0026$	$4.3418 \pm 0.0032$
13	$0.9692 \pm 0.0026$	$1.6122 \pm 0.0102$	$0.00226 \pm 0.00268$	$0.2059 \pm 0.0092$	$2.0613 \pm 0.0027$	$4.3792 \pm 0.0034$

### 3.5. Discussion

Let us show in Figure 12 the effective dimension versus  $N_z$ . As seen, though  $d_{\text{eff}}$  deviates systematically from  $d = 2$ , its values are however very close to 2. This means that the 2D character is dominant even at  $N_z = 13$ .

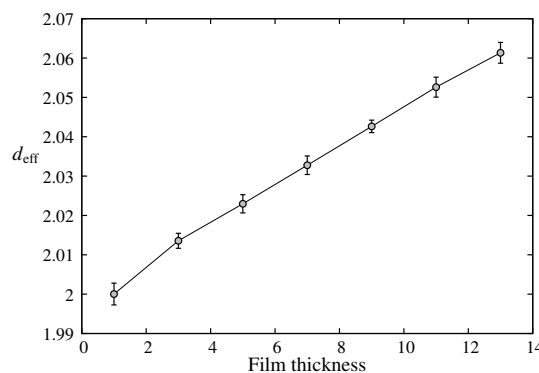


**Figure 12.** Effective dimension  $d_{\text{eff}}$  of thin film defined by  $d_{\text{eff}}\nu = 2 - \alpha$ , as a function of thickness. See text for comments.

As mentioned above,  $d_{\text{eff}}$  is very close to 2. However,  $T_c(L = \infty, N_z)$  increases very fast to reach a value close to  $T_c$  of the 3D Ising model ( $\simeq 4.51$ ) at  $N_z = 13$ . This is an interesting point. In Ref. [12] Capehart and Fisher define the critical-point shift as

$$\varepsilon(N_z) = [T_c(L = \infty, N_z) - T_c(3D)] / T_c(3D) \quad (16)$$

They showed that

$$\varepsilon(N_z) \approx \frac{b}{N_z^{1/\nu}} [1 + a/N_z] \quad (17)$$

where  $\nu = 0.6289$  (3D value). Using  $T_c(3D) = 4.51$ , we fit the above formula with  $T_c(L = \infty, N_z)$  taken from Table 1, we obtain  $a = -1.37572$  and  $b = -1.92629$ .

Our results and the fitted curve are shown in Figure 13. Note that the correction factor  $[1 + a/N_z]$  is necessary to obtain a good fit for small  $N_z$ . The prediction of Capehart and Fisher is verified by our result.

If the cross-over dimension raised by Capehart and Fisher [12] is identified with the effective dimension between 2 and 3, then the hyperscaling relation involving the space dimension  $d$  cannot be satisfied in the case of thin films. Let us take the case  $N_z = 13$ , we have  $d\nu = 2 \times 0.9692 = 1.9384$ , while  $2 - \alpha = 2 - 0.00226 = 1.99774$  far from the  $d\nu$  value. The hyperscaling relation is thus violated.

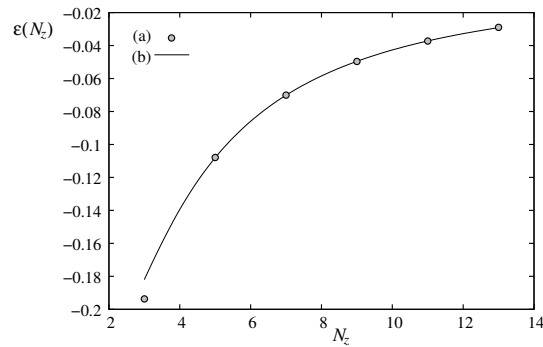


**Figure 13.** Critical temperature at infinite  $L$ ,  $T_c(L = \infty, N_z)$ , versus  $N_z$ . MC results are shown by points, continuous line is the prediction of Capehart and Fisher, Eq. (17). The agreement is excellent.

We show now that the free boundary condition in the  $z$  direction gives the same result, within errors, as the periodic boundary condition (PBC), as far as the critical exponents are concerned. This is shown in Figures 14 and 15.

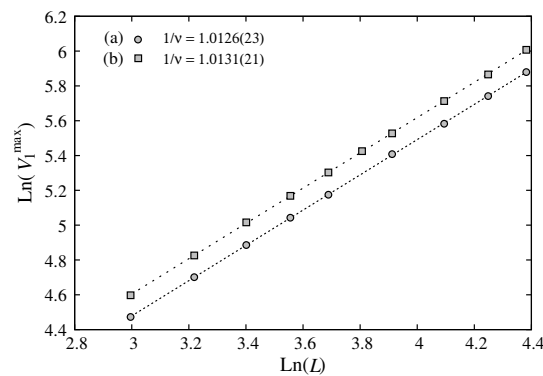


**Figure 14.** Maximum of  $V_1$  versus  $L$  in the  $\ln - \ln$  scale for  $N_z = 5$ : (a) without PBC in  $z$  direction (b) with PBC in  $z$  direction. The slopes are indicated on the figure.

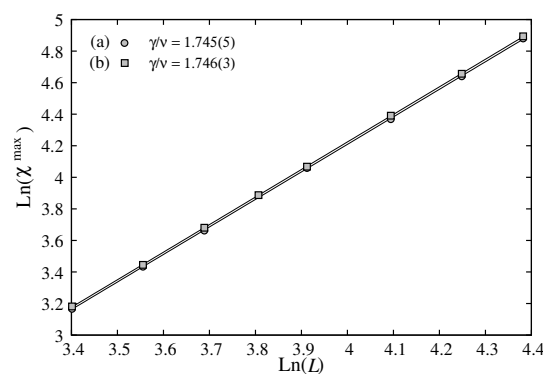


**Figure 15.**  $\chi^{\max}$  versus  $L$  in the  $\ln - \ln$  scale for  $N_z = 5$  (a) without PBC in  $z$  direction (b) with PBC in  $z$  direction. The data points of two cases are not distinguishable in the figure scale. The slopes are indicated on the figure.

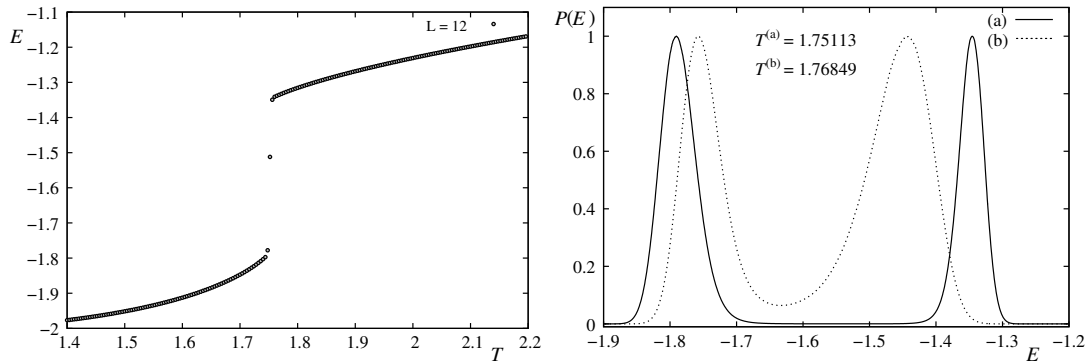
We would like to emphasize that the Rushbrooke inequality  $\alpha + 2\beta + \gamma \geq 2$  is verified within errors as an equality for each  $N_z$  as seen in Table 1.

#### 4. Cross-Over from First- to Second-Order Transition with Varying Film Thickness

In this section, we show that the film thickness can alter the nature of the transition. We cite here our work on the cross-over between the first- and second-order transition when the film thickness of a fully frustrated FCC antiferromagnet with Ising spins is decreased to  $\leq 4$  layers (two FCC cells). We

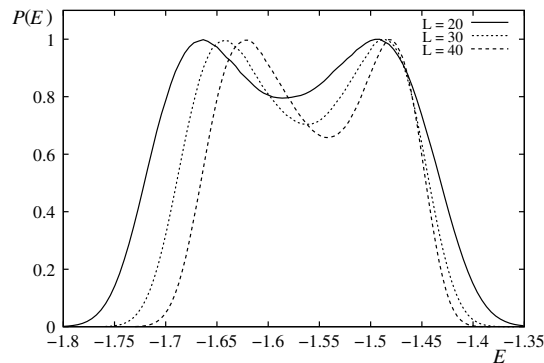
used the highly-efficient Wang-Landau method [21–27] to detect the thickness where the first-order transition becomes of second-order.

Figure 16 shows the strong first-order character of the transition with an energy discontinuity in the bulk case.



**Figure 16.** (a) Energy of the bulk case vs  $T$  for  $L \times L \times L = 12^3$  FCC cells, i. e. the number of spins is  $4L^3$ ; (b) Energy histogram with periodic boundary conditions in all three directions (continuous line) and without PBC (dotted line) in  $z$  direction. The histogram was recorded at the transition temperature  $T_c$  for each case (indicated on the figure).

In the case of a thin film composed of 8 layers ( $N_z=4$  FCC cells in the  $z$  direction), the first-order character remains as shown in Figure 17 with a double-peak structure.



**Figure 17.** Energy histogram for  $L = 20, 30, 40$  with film thickness of 8 atomic layers at  $T = 1.8218, 1.8223, 1.8227$ , respectively.

When we decrease the film thickness, the latent heat goes to zero at 4 layers (i. e.  $N_z = 2$ ) as shown in Figure 18.

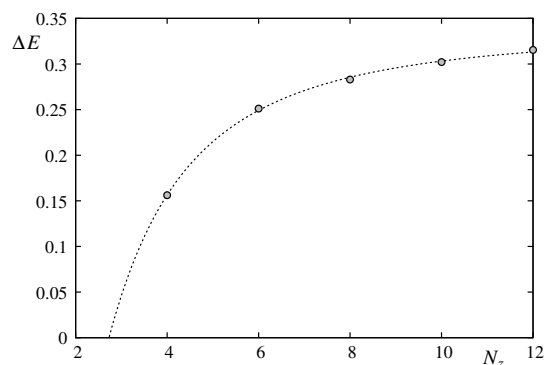


**Figure 18.** The latent heat  $\Delta E$  as a function of thickness  $L_z = 2N_z$  (points are MC results). The latent heat goes to zero at  $N_z = 2$ , i.e. at  $L_z = 4$  atomic layers. The continuous line is the fitted function Eq. (18).

We have fitted  $\Delta E$  with the following function

$$\Delta E = A - \frac{B}{N_z^{d-1}} \left[ 1 + \frac{C}{N_z} \right], \quad (18)$$

where  $d = 3$  is the space dimension,  $A = 0.3370$ ,  $B = 3.7068$ ,  $C = -0.8817$ . The second term in the brackets corresponds to a size correction. As seen in Figure 18, the latent heat vanishes at a thickness  $L_z = 2N_z = 4$ . This is verified by our simulations for a 4-layer film: the transition has a continuous energy across the transition region, even when  $L = 150$ .

The energy versus  $T$  for  $L_z = 4$  is shown in Figure 19.

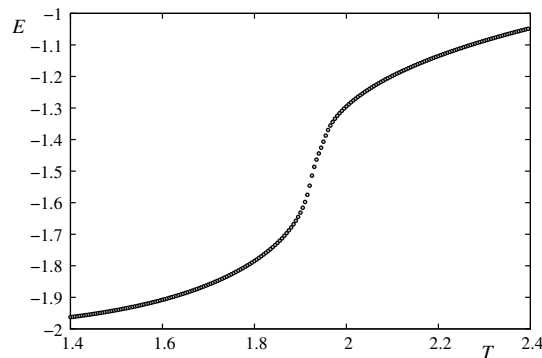


**Figure 19.** Energy versus temperature  $T$  for  $L = 120$  for a 4-layer film.

As seen in Figure 20, there are two close transitions: transition of the surface layers at  $z = 0$  and  $z = 3/2$ , and that of the beneath layers at  $z = 1/2$  and  $z = 1$  (the lattice constant is taken to be 1).

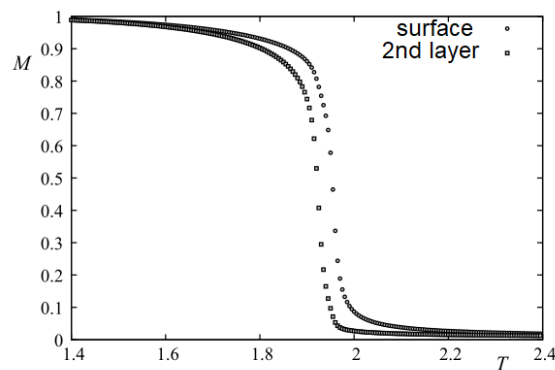


**Figure 20.** Layer magnetizations for  $L = 120$  with a 4-layer film: the higher (lower) curve is the surface (beneath) layer magnetization.

The surface layer has larger magnetization than that of the second layer unlike the non-frustrated case shown in the previous section. One can explain this by noting that due to the lack of neighbors, surface spins are less frustrated than the interior spins, making them more stable than the interior spins. This has been found at the surface of the frustrated helimagnetic film [17]. In order to find the nature of these transitions, using the Wang-Landau technique we study the finite-size effects which are shown in in Figures 21 and 22. The first peak at  $T_1 \simeq 1.927$  corresponds to the vanishing of the second-layer magnetization, it does not depend on the lattice size, while the second peak at  $T_2 \simeq 1.959$ , corresponding to the disordering of the two surface layers, it depends on  $L$ . The histograms shown in Figure 23 are taken at and near the transition temperatures show a Gaussian distribution indicating a non first-order transition.

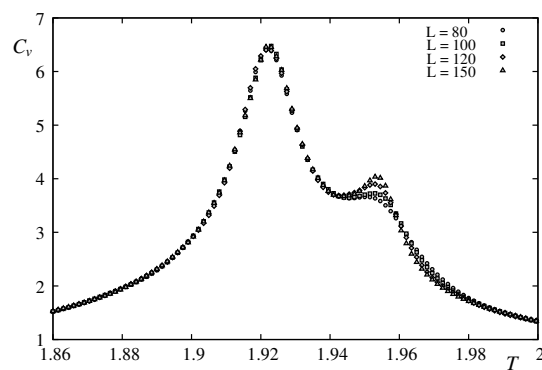


**Figure 21.** Specific heat are shown for various linear  $xy$  plane sizes  $L$  versus  $T$  for a 4-layer film.

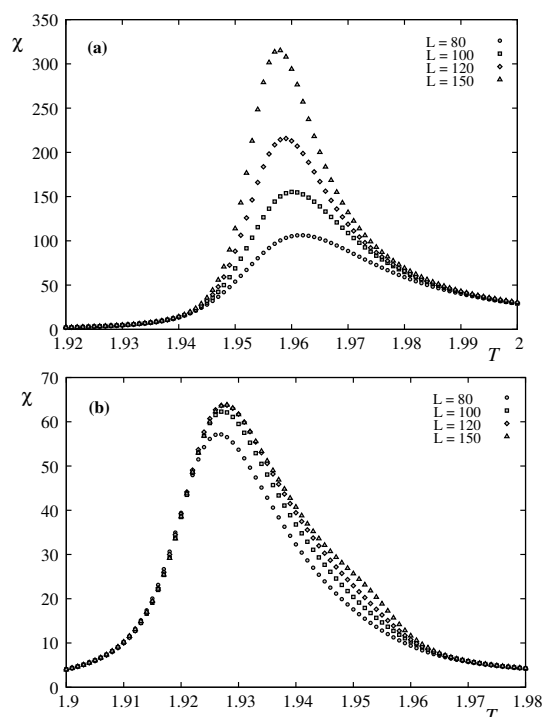


**Figure 22.** Susceptibilities of the first layer (a) and the second layer (b) are shown for various sizes  $L$ , versus  $T$  in a 4-layer film.

The fact that the peak at  $T_1$  of the specific heat does not depend on  $L$  suggests two scenarios: i)  $T_1$  does not correspond to a transition, ii)  $T_1$  is a Kosterlitz-Thouless transition. We are interested here to the size-dependent transition at  $T_2$ . Using the multi-histogram technique, we have obtained  $\nu = 0.887 \pm 0.009$  and  $\gamma = 1.542 \pm 0.005$  for the case of 4 layers (see Figures 24 and 25). These values do not correspond neither to 2D nor 3D Ising models  $\nu(2D) = 1$ ,  $\gamma(2D) = 1.75$ ,  $\nu(3D) = 0.63$ ,  $\gamma(3D) = 1.241$ . We can interpret this as a dimension cross-over between 2D and 3D. Note that the values we have obtained  $\nu = 0.887 \pm 0.009$  and  $\gamma = 1.542 \pm 0.005$  belong to a new, unknown universality class.

At the time of our work [28], we relied on the hyperscaling relation with  $d = 2$  to deduce critical exponent  $\alpha$  and using the Rushbrooke equality to calculate  $\beta$ . However, in view of a possible violation of the hyperscaling when  $d$  is not the space dimension, we cannot conclude without a direct calculation of  $\alpha$  as we have done in the previous section.

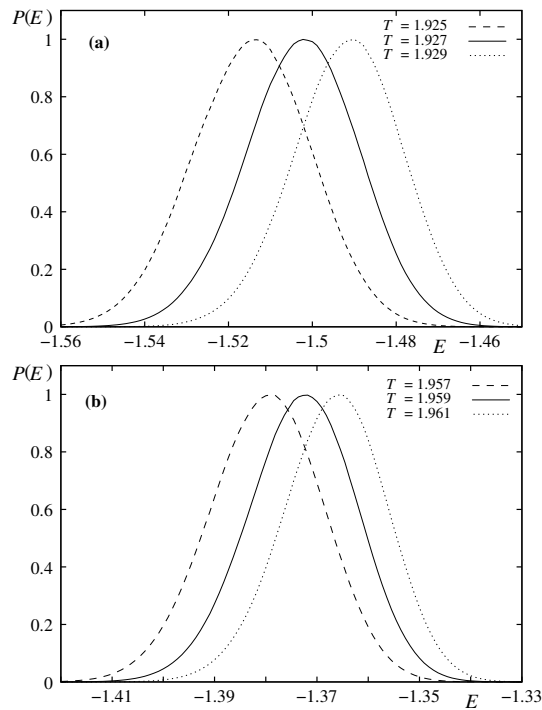


**Figure 23.** Energy histograms recorded at temperatures (indicated on the figure) corresponding to the the first (a) and second (b) peaks observed in the specific heat, for  $L = 120$  with 4-layer film thickness  $L_z = 4$ .

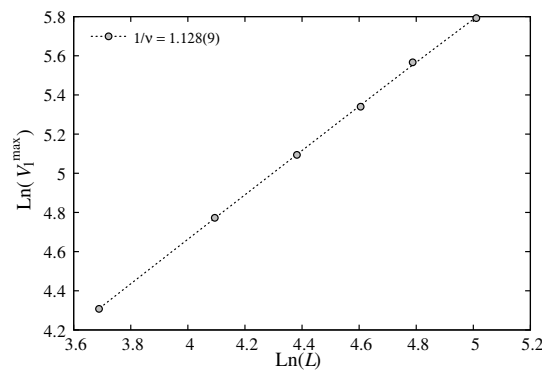


**Figure 24.** The maximum value of  $V_1$  as a function of  $L$  in the  $\ln - \ln$  scale. The slope of this straight line gives  $1/\nu$ . See the value of  $\nu$  in the text.

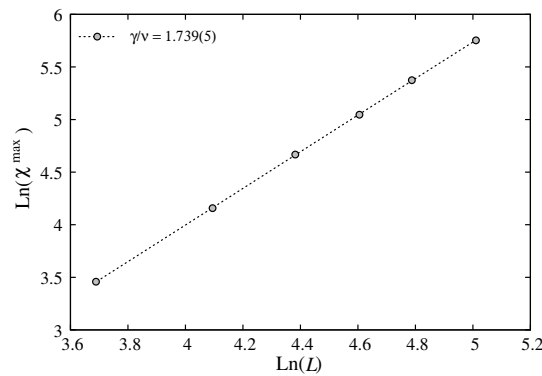


**Figure 25.** The maximum of the susceptibility  $\chi^{\max}$  as a function of  $L$  in the  $\ln - \ln$  scale. The slope of this straight line gives  $\gamma/\nu$ . See the value of  $\gamma$  in the text.

## 5. Other Cases Violating the Hyperscaling Relation?

There are cases where the systems have an additional degree of freedom distinct from the order parameter. This is the case of XY spins with a chirality symmetry: while the chiral symmetry can be mapped onto an Ising-like symmetry, the continuous nature of XY spins affects the criticality of the Ising symmetry breaking. Another case is a system of Ising spins in which each spin moves around its lattice site, a kind of magneto-elastic coupling. These two cases have been previously studied [29–31]. We briefly review these results below under the view angle of new universality class and the violation or not of the hyperscaling relation below  $d_u = 4$ .

### 5.1. Fully Frustrated XY Square Lattice

The fully frustrated with XY spins on the square lattice has been intensively studied [29,32–39]. The lattice with the ground-state (GS) spin configuration is shown in Figure 26 (see [32]) where the angles between spins linked by a ferromagnetic (antiferromagnetic) bond is  $\pi/4$  ( $3\pi/4$ ) with right and left chiralities. This GS is equivalent to an Ising model on an antiferromagnetic square lattice. When  $T$  increases, one expects a transition of the Ising type. However, at finite  $T$ , the XY spins fluctuate around their GS orientations shown in Figure 26, making the nature of the phase transition more complex as seen below. Note that some authors have claimed that there are two separate transition of XY and Ising natures [36–39]. However, our results [29] and those of Refs. [34,35] show clearly that there is only a single transition of the new criticality called "coupled XY-Ising" universality class. We show below our results.

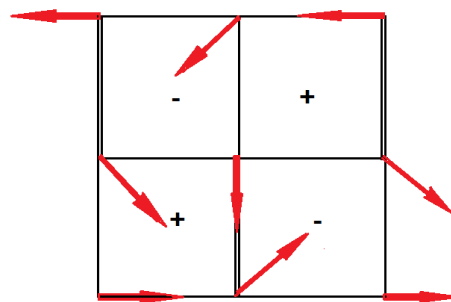


**Figure 26.** The square lattice: single (double) bonds are ferromagnetic (antiferromagnetic) bonds. The GS spin configuration is shown by red arrows. The right and left chiralities are denoted by "+" and "-".

In Ref. [29], using the highly-precise multi-histogram MC simulations described above, we have obtained the critical exponents  $\nu$  and  $\gamma$ . We show in Figure 27 the Binder energy cumulant  $U_E$  [8,9] as a function of  $L$ : as seen the curve approaches asymptotically  $2/3$  from below. This indicates a second-order nature of the transition.

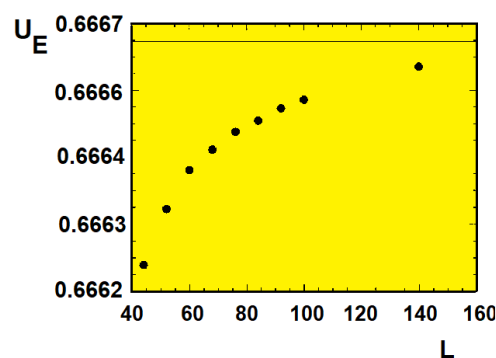


**Figure 27.** The Binder energy cumulant  $U_E$  versus  $L$  calculated at  $T_c(L = \infty) = 0.4552(2)$ . The horizontal line indicates  $U_E(L = \infty) = 2/3$ . The results show that the transition is of second order.

Let us show the susceptibility versus  $T$  for  $L = 44, 52, 60, 84, 100, 140$  in Figure 28. A single peak for each size indicates a single transition as said above. For  $L = 140$  the peak is very close to  $T_c(L = \infty) = 0.45522(2)$  estimated using Eq. (13) and  $\nu = 0.852(2)$  calculated below using the maxima of  $V_1$  and  $V_2$  shown in Figure 29. The fitting error is less than 0.1%. Note that our value is the same as that of Ref. [35] which used the same multi-histogram MC technique, but differs from those obtained by less efficient methods ( $\nu = 0.816$  in Ref. [38] and  $\nu = 0.889$  in Ref. [39] for XY transition).

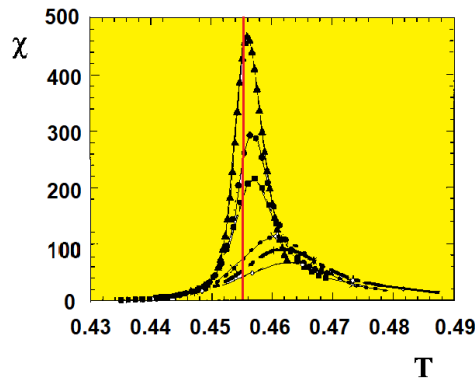


**Figure 28.** Susceptibility  $\chi$  versus  $T$  for sizes  $L = 44, 52, 60, 84, 100, 140$  (from lowest to highest curves). The red vertical line is the position of  $T_c(L = \infty)$  calculated with Eq. (TCL) using  $\nu$  obtained by Figure 29 below.

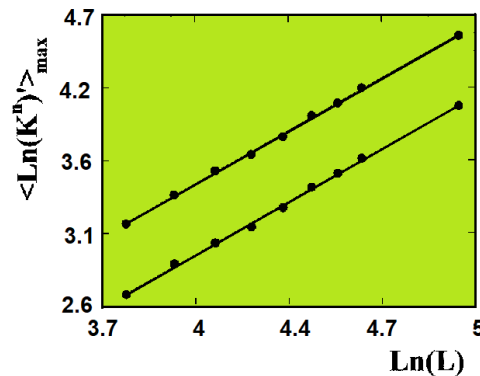


**Figure 29.** The maximum of cumulants  $V_1$  and  $V_2$  versus size  $L = 44, 52, 60, 84, 100, 140$  in the  $\ln - \ln$  scale. The slopes give the same  $1/\nu$ . See text for the value of  $\nu$ .

We calculate exponent  $\gamma$  using the peak values of  $\chi$  for varying  $L$ . The curve in the  $\ln - \ln$  scale is shown in Figure 30. The slope gives  $\gamma/\nu$ . Using  $\nu = 0.852$  we obtain  $\gamma = 1.531(3)$  which is different from  $1.448(24)$  obtained by Ref. [38].

At the time of our work in Ref. [29], we did not calculate  $\beta$  and  $\alpha$  as we have done on thin films presented in the precedent section. We were confident on the hyperscalings  $d\nu = \gamma + 2\beta$  and  $\alpha = 2 - d\nu$ , so we used these relations to calculate  $\beta$  and  $\alpha$ . However, in view of the question whether or not these relations are valid in particular cases such as the case of thin films shown in Section 2 and the double transition in the case of fully frustrated square lattice presented here, we would like to check the validity of the hyperscaling relations. We can use  $\nu$  and  $\gamma$  obtained here and the value of  $2\beta/\nu = 0.31(3)$  obtained in Ref. [35], then we have  $d\nu = 2 \times 0.852 = 1.704$  while  $\gamma + 2\beta = 1.531 + 0.31 \times 0.852 = 1.795$ . We see that  $d\nu < \gamma + 2\beta$  even if we take into account errors of the exponents. Note that in these estimations we have used the Rushbrooke "equality" which is so far verified within errors in all known cases.

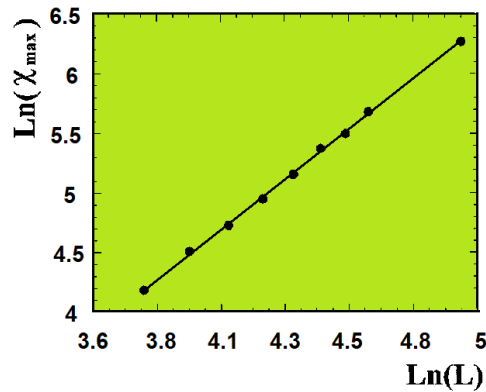


**Figure 30.** The maximum of susceptibility  $\chi$  versus size  $L = 44, 52, 60, 84, 100, 140$  in the  $\ln - \ln$  scale. The slope indicates the value of  $\gamma/\nu$ . See text for the value of  $\gamma$ .

We note that it has been found in Ref. [35] by direct FSS that  $\alpha/\nu = 0.48(7)$ . Using  $\nu = 0.852$  obtained by us and by Ref. [35], one obtains  $\alpha \simeq 0.409$ . This yields  $2 - \alpha = 2 - 0.409 = 1.591$  which is not equal to  $d\nu = 2 \times 0.852 = 1.704$  (here we do not use the Rushbrooke equality).

The conclusion for this coupled XY-Ising model based on the high-precision multi-histogram technique of our work and of Ref. [35] is that the hyperscaling relation is violated.

### 5.2. Effect of Magneto-Elastic Coupling on Criticality

There are certainly other exotic models which may violate the hyperscaling relation for  $d < 4$ . One of these is the magneto-elastic coupling model that we have studied by using the multi-histogram technique [30,31]. The model consists of atoms on a stacked triangular lattice. Each atom carries an Ising spin and moves around its lattice equilibrium position. There are two kinds of interaction which are distance-dependent: the elastic interaction between atoms and the magnetic interaction between Ising spins. We suppose the following Hamiltonian:

$$\mathcal{H} = U_0 \sum_{ij} J(r_{ij}) + U_m \sum_{ij} J(r_{ij}) \sigma_i \sigma_j \quad (19)$$

where the first sum is the elastic interaction with amplitude  $U_0$ , and the second sum expresses the interacting spins with amplitude  $U_m$ . The distance-dependence is supposed to be the Lennard-Jones potential

$$J(r_{ij}) = (r_0/r_{ij})^{12} - 2(r_0/r_{ij})^6 \quad (20)$$

where  $r_0 = 1$  is the distance at equilibrium between NN in the triangular planes and also in the stacking direction.,  $r_{ij} = r_i - r_j$  is the instantaneous distance between NN.

In order to separate the spin disordering from the melting, we take the ratio  $Q = U_0/U_m$  large enough so that the magnetic transition occurs at low  $T$ . The cut-off distance is taken as  $r_c = 1.366r_0$ .

Simulations using multiple-histogram technique have been performed. The reader is referred to Ref. [30,31] for details. We just summarize the results in Table 2. Note that we have calculated at the time of our work (Ref. [30,31]) only  $\nu$  and  $\gamma$ , and we have relied on the hyperscaling relations  $d\nu = 2 - \alpha$  and  $\gamma/\nu = 2 - \eta$  to calculate  $\alpha$  and  $\eta$  listed in Table 2. However, we believe that if  $\alpha$  is directly calculated as in section 2, the result of  $\alpha$  may be different, due to the mixing of elastic and magnetic interactions. The nature of the transition depends on  $Q$ : it changes from the Ising nature at large  $Q$  to close to the XY universality class as seen in Table 2. In such complex situations, we are not sure that the hyperscaling relations are valid. Further direct calculations of  $\alpha$  in the way we did in Ref. [11] are necessary to conclude on this point.

**Table 2.** Critical exponents obtained by multi-histogram technique for different  $Q$ .  $a$ : Results from Ref. [40],  $b$ : Results from Ref. [41]

$Q$	$\alpha$	$\beta$	$\nu$	$\gamma$	$\eta$
8	0.140(1)	0.310(1)	0.620(5)	1.245(5)	-0.01(1)
5	0.141(5)	0.301(5)	0.620(5)	1.259(5)	-0.03(1)
4	0.135(6)	0.308(5)	0.622(5)	1.249(5)	-0.01(1)
3D Ising	0.1070( $a$ )	0.3265( $b$ )	0.6305( $b$ )	1.2390( $b$ )	0.0370( $b$ )
3	-0.024(4)	0.353(5)	0.675(5)	1.314(5)	0.053(5)
3D XY	-0.0100( $a$ )	0.3455( $b$ )	0.671( $b$ )	1.3150( $b$ )	0.040( $b$ )

## 6. Concluding Remarks

We know that the hyperscaling relation is verified in  $d = 3$  for Ising, XY and Heisenberg spins (results of highly-efficient simulations), and in  $d = 2$  for Ising spins (exact results). However, as shown in this review, there are particular cases that the hyperscaling relation  $d\nu = 2 - \alpha$  is violated. One of these situations is the case of a magnetic thin film with small thickness. Another case is the fully frustrated XY square lattice where we show that there is a single phase transition of a new coupled XY-Ising universality: the results of Ref. [35] and our results using the same method of simulation (multiple-histogram technique) are the same for  $\nu$  and  $\gamma$ . We did not calculate  $\beta$ , but we believe we should obtain the same  $\beta$  obtained in Ref. [35] in view of the same results obtained for  $\nu$  and  $\gamma$ . The hyperscaling relation is then violated in this case. The case of a system with a magneto-elastic interaction shows a new universality class. The violation, or not, of the hyperscaling relation in this case needs further verifications.

To conclude, let us emphasize that, in view of the precise values we have obtained, at least for thin films, the hyperscaling relation is not verified. We have also presented evidence of the violation of the hyperscaling relation in some other cases. We believe that more cases should be studied before a general conclusion could be drawn. This explains the question mark in the title of this review.

**Acknowledgments:** The authors are grateful to X.-T. Pham-Phu and the late E. H. Boubcheur for participating in some works cited in this paper.

**Funding:** This research received no external funding.

**Conflicts of Interest:** The authors declare no conflict of interest.

## References

1. Diep, H. T. *Theory of Magnetism*, World Scientific, World Scientific: Singapore, 2014.
2. Baxter, R. J. *Exactly Solved Models in Statistical Mechanics*, Academic Press Limited, London (U.K.) 1982.
3. Wilson, K. G. Renormalization Group and Critical Phenomena. I. Renormalization Group and the Kadanoff Scaling Picture *Phys. Rev. B* **1971** *4*, 3174.
4. Wilson, K. G. Renormalization Group and Critical Phenomena. II. Phase-Space Cell Analysis of Critical Behavior *Phys. Rev. B* **1971** *4*, 3184.
5. Cardy, J. *Scaling and renormalization in statistical physics*, Cambridge University Press: Cambridge (U.K.), 1996.
6. Young, A. P. Violations of Hyperscaling in Finite-Size Scaling above the Upper Critical Dimension, *Entropy* **2024** *26*(6), 509; <https://doi.org/10.3390/e26060509> (this present Special Issue: Violations of Hyperscaling in Phase Transitions and Critical Phenomena—in Memory of Prof. Ralph Kenna).
7. Honchar, Yu.; Berche, B.; Holovatch, Yu.; Kenna, R. When correlations exceed system size: finite-size scaling in free boundary conditions above the upper critical dimension, *Condensed Matter Physics* **2024**, *27*, 13603:1-15.
8. Ferrenberg, A. M.; Swendsen, R. H. New Monte Carlo technique for studying phase transitions, *Phys. Rev. Lett.* **1988** *61*, 2635. Erratum *Phys. Rev. Lett.* **1989** *63*, 1658.
9. Ferrenberg, A. M.; Swendsen, R. H. Optimized Monte Carlo data analysis, *Phys. Rev. Lett.* **1989** *63*, 1195.
10. A. Bunker, A.; Gaulin, B. D.; Kallin, C. Multiple-histogram Monte Carlo study of the Ising antiferromagnet on a stacked triangular lattice, *Phys. Rev. B* **1993** *48*, 15861-15872.

11. Pham-Phu, X.-T.; Ngo, V.-Thanh; Diep, H. T. Critical behavior of magnetic thin films, *Surface Science* **2009** *603*, 109–116.
12. Capehart, T. W.; Fisher, M. E. Susceptibility scaling functions for ferromagnetic Ising thin films, *Phys. Rev. B* **1976** *13*, 5021-5038.
13. Binder, K. The Monte Carlo Method for the Study of Phase Transitions: A Review of Some Recent Progress, *J. of Computational Physics* **1985** *59*, pp. 1-55.
14. Ferrenberg, A.M.; Landau, D.P. Critical behavior of the three-dimensional Ising model: A high-resolution Monte Carlo study, *Phys. Rev. B* **1991** *44*, 5081-5091.
15. Diep, H. T.; Levy, J.C.S.; Nagai, O. Effects of Surface Spin Waves and Surface Anisotropy in Magnetic Thin Films at Finite Temperatures, *Phys. Stat. Solidi (b)* **1979** *93*, 351-361.
16. Diep, H.T. Temperature-Dependent Surface Magnetization and Critical Temperature of Ferromagnetic Thin Films, *Phys. Stat. Solidi (b)* **1981**, *103*, 809-815.
17. Diep, H. T. Quantum theory of helimagnetic thin films, *Phys. Rev. B* **2015** *91*, 014436 (12 pp.).
18. El Hog, S.; Diep, H. T.; Puzskarski, H. Theory of magnons in spin systems with Dzyaloshinskii–Moriya interaction, *J. Phys.: Condens. Matter* **2017** *29* 305001 (10pp.).
19. Sharafullin, I.; Kharrasov, M. Kh.; Diep, H. T. Dzyaloshinskii–Moriya interaction in magnetoferroelectric superlattices: Spin waves and skyrmions, *Phys. Rev. B* **2019** *99*, 214420 (14 pp.).
20. Schilbe, P.; Siebentritt, S.; and Rieder, K. H. Monte Carlo calculations on the dimensional crossover of thin Ising films *Phys. Lett. A* **1996** *216*, 20-25.
21. Wang, F.; Landau, D.P. Efficient, Multiple-Range Random Walk Algorithm to Calculate the Density of States, *Phys. Rev. Lett.* **2001** *86*, 2050-2053.
22. Brown, G.; Schulhess, T. C. Wang–Landau estimation of magnetic properties for the Heisenberg model, *J. Appl. Phys.* **2005** *97*, 10E303.
23. B. J. Schulz, B. J.; Binder, K.; Müller, M.; Landau, D.P. Avoiding boundary effects in Wang-Landau sampling, *Phys. Rev. E* **2003** *67*, 067102 (2 pp.).
24. Malakis, A.; Martinos, S.S.; Hadjiagapiou, I.A.; Fytas, N.G.; Kalozoumis, P. Entropic sampling via Wang-Landau random walks in dominant energy subspaces, *Phys. Rev. E* **2005** *72*, 066120 (11 pp.).
25. Ngo, V. T.; Diep, H.T., Phase Transition in Heisenberg Stacked Triangular Antiferromagnets: End of a Controversy, *Phys. Rev. E* **2008** *78*, 031119.
26. Ngo, V.T.; Diep, H. T. Stacked Triangular XY Antiferromagnets: End of a Controversial Issue on the Phase Transition, *J. Appl. Phys.* **2008** *103*, 07C712.
27. Ngo, V.T. ; Hoang, D.-Tien; Diep, H. T. First-Order Transition in XY Fully Frustrated Simple Cubic Lattice, *Phys. Rev. E* **2010** *82*, 041123 (5 pages).
28. Pham-Phu, X. T.; Ngo, V. T.; Diep, H. T. Cross-Over from First- to Second-Order Transition in Frustrated Ising Antiferromagnetic Films, *Phys. Rev. E* **2009** *79*, 061106 (8 pp.).
29. Boubcheur, E. H.; Diep, H. T. Critical behavior of the two-dimensional fully frustrated XY model, *Phys. Rev. B* **1998** *58*, 5163-5165.
30. Boubcheur, E. H.; Diep, H. T. Effect of elastic interaction on critical behavior of three-dimensional Ising model, *J. Appl. Physics* **1999** *85*, 6085-6087.
31. Boubcheur, E. H.; Massimino, P.; Diep, H. T. Effects of magnetoelastic coupling: critical behavior and structure deformation, *Journal of Magnetism and Magnetic Materials* **2001** *223*, 163-168.
32. Berge, B.; Diep, H. T. ; Ghazali, A.; Lallemand, P. Phase transitions in two-dimensional uniformly frustrated XYspin systems, *Phys. Rev. B* **1986** *34*, 3177-3184.
33. Granato, E.; Nightingale, M. P. Chiral exponents of the square-lattice frustrated XY model: a Monte Carlo transfer-matrix calculation, *Phys. Rev. B* **1993** *48*, 7438-7444.
34. Lee, J.; Kosterlitz, J. M.; Granato, E. Monte Carlo study of frustrated XY models on a triangular and square lattice, *Phys. Rev. B* **1991** *43*, 11531-11534.
35. Granato, E.; Kosterlitz, J.M.; Lee, J.; Nightingale, M. P. Phase transitions in coupled XY-Ising systems, *Phys. Rev. Lett.* **1991** *66*, 1090-1093.
36. Olsson, P. Two Phase Transitions in the Fully Frustrated XY Model, *Phys. Rev. Lett.* **1995** *75*, 2758-2761.
37. Jeon, G. S.; Park, S. Y.; Choi, M. Y. Double transitions in the fully frustrated XY model, *Phys. Rev. B* **1997** *55* 14088-14091.
38. Lee, S. ; Lee, K.C. Phase transitions in the fully frustrated XY model studied with use of the microcanonical Monte Carlo technique, *Phys. Rev. B* **1994** *49*, 15184-15189.

39. Ramirez-Santiago, G; Jose, J. V. Critical exponents of the fully frustrated two-dimensional XY model, *Phys. Rev. B* **1994** *49*, 9567-9582.
40. Antenonko, S. A.; Sokolov, A. I. Critical exponents for a three-dimensional  $O(n)$ -symmetric model with  $n > 3$ , *Phys. Rev. E* **1995** *51*, 1894-1898.
41. Le Guillou, J. C.; Zinn-Justin, J. Accurate critical exponents from the  $\epsilon$ -expansion, *J. Phys. (France) Lett.* **1985** *46*, L137-141.

**Disclaimer/Publisher's Note:** The statements, opinions and data contained in all publications are solely those of the individual author(s) and contributor(s) and not of MDPI and/or the editor(s). MDPI and/or the editor(s) disclaim responsibility for any injury to people or property resulting from any ideas, methods, instructions or products referred to in the content.